International Tables for Crystallography (2006). Vol. F, Section 11.5.8, p. 241.

11.5.7.6. *Anomalous dispersion*

The quality of anomalous-dispersion data can be assessed by calculation of the average scatter, expression (11.5.6.6). The ratios $\langle\sigma_{Ih}\rangle/\langle\sigma^{+}_{Ih}\rangle$ and $\langle\sigma_{Ih}\rangle/\langle\sigma^{-}_{Ih}\rangle$ should be larger than unity for significant anomalous data (Fig. 11.5.7.8). Note the much larger ratios for the scatter among measurements of I_h for data measured at the absorption edge of Se, as opposed to measurements remote from the edge. The decreasing values of the ratios with resolution are due to the decrease of I_h value, thus causing the error in the measurement of I_h to approach the difference in intensity of Bijvoet opposites.

11.5.8. Conclusions

The generalized HRS method allows scaling and averaging of X-ray diffraction data collected with an oscillation camera while simultaneously using full and partial reflections. The procedure is as useful for thin slices of reciprocal space as it is for thicker slices.

The results of data processing with the two different algorithms indicate that method 1, based on adding partial reflections, may fail to scale data sets with gaps in the rotation range or with low redundancy. The values of the scale factors obtained with both methods are similar, except for cases where there are gaps in the rotation range or dramatic changes in the true scale factors between consecutive frames. In these cases, method 1 produces a physically wrong result. The algorithm used by method 1 is probably similar to that used by *SCALEPACK* (Otwinowski & Minor, 1997).

Method 2 is more stable and versatile than method 1, and allows the scaling of data sets with incompletely measured reflections and low redundancy. The major drawback of method 2 is that errors in the crystal orientation matrix and mosaicity, as well as inadequacies of the theoretical model for reflection partiality, contribute to errors in the scaled intensities. Therefore, post refinement is needed for method 2 to perform at its best.

Appendix 11.5.1.

Partiality model (Rossmann, 1979; Rossmann *et al.*, 1979)

Small differences in the orientation of domains within the crystal, as well as the cross fire of the incident X-ray beam, will give rise to a series of possible Ewald spheres. Their extreme positions will subtend an angle $2m$ at the origin of the reciprocal space, and their centres lie on a cusp of limiting radius $\delta = m/\lambda$, where m is the half-angle effective mosaic spread. As the reciprocal lattice is rotated around the axis (Oy) perpendicular to the mean direction of the incident radiation (Oz), a point P will gradually penetrate the effective thickness of the reflection sphere (Fig. A11.5.1.1). Initially, only a few domain blocks will satisfy Bragg's law, but upon further rotation the number of blocks that are in a reflecting condition will increase. The maximum will be reached when the point P has penetrated halfway through the sphere's effective thickness, after which there will be a decline of the crystal volume able to diffract.

Let q be a measure of the fraction of the path travelled by P between the extreme reflecting positions P_A and P_B, and let p be the fraction of the energy already diffracted. Then the relation between p and q must have the general form shown in Fig. A11.5.1.2. It is physically reasonable to assume that the curve for p is tangential to $q = 0$ at $p = 0$ and to $q = 1$ at $p = 1$.

A reasonable approximation to the above conditions can be obtained by considering the fraction of the volume of a sphere removed by a plane a distance q from its surface (Fig. A11.5.1.2). It is easily shown that if p is the volume, then

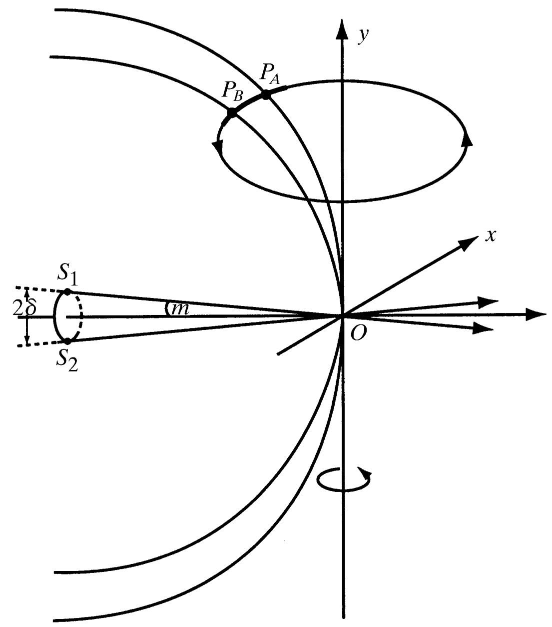

Fig. A11.5.1.1. Penetration of a reciprocal-lattice point P into the sphere of reflection by rotation around Oy. The extremes of reflecting conditions at P_A and P_B are equivalent to X-rays passing along the lines S_1O and S_2O with centres of the Ewald spheres at S_1 and S_2 and subtending an angle of $2m$ at O. Hence, in three dimensions, the extreme reflecting spheres will lie with their centres on a circle of radius $\delta = m/\lambda$ at $z = -1/\lambda$.

$$p = 3q^2 - 2q^3. \qquad \text{(A11.5.1.1)}$$

This curve is shown in Fig. A11.5.1.2 and corresponds to assuming that the reciprocal-lattice point is a sphere of finite volume cutting an infinitely thin Ewald sphere. Also shown in Fig. A11.5.1.2 is the line $p = q$ which would result if the reciprocal-lattice point were a rectangular block whose surfaces were parallel and perpendicular to the Ewald sphere at the point of penetration.

Assuming a right-handed coordinate system (x, y, z) in reciprocal space fixed to the camera, it is easily shown (Wonacott, 1977) that the condition for reflection is

$$d^{*2} + (2z/\lambda) = 0, \qquad \text{(A11.5.1.2)}$$

where d^* is the distance of a reciprocal-lattice point $P(x, y, z)$ from the origin, O, of reciprocal space. Similarly, it can be shown that at the ends of the path of the reciprocal-lattice point through the finite thickness of the sphere,

$$\begin{aligned} &d^{*2} + \delta^2 + (2z/\lambda) - 2\delta\left(x_A^2 + y_A^2\right)^{1/2} = 0 \quad \text{and} \\ &d^{*2} + \delta^2 + (2z/\lambda) - 2\delta\left(x_B^2 + y_B^2\right)^{1/2} = 0. \end{aligned} \qquad \text{(A11.5.1.3)}$$

Therefore,

$$\begin{aligned} z_A &= (\lambda/2)\left[-d^{*2} - \delta^2 + 2\delta\left(x_A^2 + y_A^2\right)^{1/2}\right], \\ z_B &= (\lambda/2)\left[-d^{*2} - \delta^2 + 2\delta\left(x_B^2 + y_B^2\right)^{1/2}\right]. \end{aligned} \qquad \text{(A11.5.1.4)}$$

Since δ is small, it can be assumed that $2\delta(x^2 + y^2)^{1/2}$ is independent of the position of the reciprocal-lattice point P between the extreme positions P_A and P_B (Fig. A11.5.1.1). Hence, the length of the path through the finite thickness of the sphere is proportional to

$$z_A - z_B = 2\lambda\delta\left(x_P^2 - y_P^2\right)^{1/2}. \qquad \text{(A11.5.1.5)}$$

references